180 nm CMOS Cold-Start Energy-Aware Switching Circuit for Energy Management in WPT Receiver

Davor VINKO, Kresimir GRGIC, Domagoj BILANDZIJA

Faculty of Electrical Engineering, Computer Science and Information Technology Osijek,
University of J. J. Strossmayer Osijek, Kneza Trpimira 2b, 31000 Osijek, Croatia

davor.vinko@ferit.hr, {kresimir.grgic, domagoj.bilandzija}@ferit.hr

Abstract. *Modern electronic devices offer high level performance at low power consumption. This opens a possibility to have battery-less electronic devices. Energy harvesting and wireless power transfer are popular methods to power such devices. Both methods require energy management. The focus of this paper is on energy management for receiver circuit in a wireless power transfer system. More specifically, the paper focuses on a cold-start energy-aware switching circuit which is a key building block of energy management in WPT receiver. Proposed integrated circuit is designed to operate in discontinuous mode and can supply power to load circuits which require higher voltage and current levels than available from the WPT receiver. Unlike most similar solutions who are fully integrated, the proposed integrated circuit uses two external trimmer resistors to adjust required voltage levels and the power consumption. External trimmer resistors also allow to compensate for the process variations of IC fabrication. Developed circuit is fabricated in 180 nm TSMC CMOS technology and evaluated through laboratory measurement. Cold-start functionality and energy-aware switching are verified through standalone measurements and measurements with WSN node powered through developed circuit. The power consumption of cold-start switching circuit is measured less than 1 μW.*

Keywords

Electronic circuit design, energy management, wireless power transfer

1. Introduction

Wireless sensor nodes offer a variety of on-board sensors, sufficient computational power and support for number of communication protocols. The only obstacle to have widespread deployment of wireless sensor nodes is their battery dependence. Energy harvesting methods are extensively researched to develop a reliable powering method for wireless sensor nodes [1]. Most common energy harvesting methods are thermoelectric generators, piezo/ vibration generators, microbial fuel cells, solar cells and micro-scale wind turbines [2], [3]. For WSNs which are e.g. built in walls, majority of energy harvesting methods in not useful (solar, wind, thermoelectric, piezo). In such applications, a resonant wireless power transmission can be used to power sensors and wireless sensor nodes.

Using energy harvesting or wireless power transmission to power WSNs requires similar approach [4]. The voltage, current and power levels generated by energy harvester or WPT receiver are not constant and can significantly change depending on environment conditions or relative position of WPT transmitter/receiver. Therefore, a mediator circuit is needed between power source (energy harvester or WPT receiver) and load circuit (wireless sensor node). This mediator circuit is commonly referred to as energy management circuit and is always used in energy harvesting systems.

Energy harvester sources can be generally divided into two categories: those that generate DC voltage (thermoelectric, solar, microbial) and those that generate AC voltage (piezo, vibration, microwind). In general, the voltage levels from energy harvester have to be increased. For DC energy harvesters boost step-up voltage converters and charge pumps are mostly used. Both require additional oscillator circuit. For AC energy harvesters, two approaches are used. The first approach uses a rectifier followed by the same topology as in DC energy harvesters. The second approach is to drive voltage multiplier or boost converter with oscillations from AC energy harvester.

Lately, there have been a number of papers discussing the cold-start circuit [8–13]. Energy harvesters such as thermoelectric and microbial fuel cells generate very low DC voltages (in the range below 100 mV). They use step-up voltage converters and storage capacitors to provide higher voltage levels needed for both energy management circuit and load circuit. The problem occurs after longer periods with no harvested energy. The charge in storage capacitor gets depleted and the control circuit, which drives step-up converter, cannot start. To cope with this problem, some energy harvesting designs use batteries to provide power supply during time intervals without harvested energy [13]. As energy harvesting systems aim to battery-less design, various cold-start circuit solutions are reported [8–12]. Cold-start circuit is used for initial start of the energy management

circuit or to restart it after longer inactive periods. It requires higher voltages to self-start, but once it starts, it can operate on significantly lower voltages [9–12].

In the use-case proposed in this paper, when energy harvester cannot continually supply the load, the energy harvesting system operates in cycles. It collects and stores harvested energy for a longer period of time, and then it powers the load circuit for a short time interval. For such operating mode, an additional building block is needed which monitors the collected energy and acts as a switch between storage capacitor and load circuit. This is the use-case we will be focusing on.

This paper presents an energy-aware switching circuit with cold-start functionality designed for a WPT receiver. The next section describes the proposed energy management topology in WPT receiver. The third section describes the design of the switching circuit. In the fourth section, the measurement results are given followed by conclusion.

2. Energy Management in WPT Receiver

Basic schematic of WPT system is given in Fig. 1. In resonant magnetic WPT system both transmitter and receiver have a resonant tank tuned to the resonant frequency of WPT system. Resonant tank is formed by an inductor and capacitor which can be connected in series or in parallel. Figure 1 shows a WPT system with a parallel resonant tank on both the transmitter and the receiver side. Resonant WPT system is characterized with low coupling coefficient k. The mutual position of the receiver and transmitter has significant impact on the coupling coefficient, which affects the maximal voltage and current available at the receiver's side.

The receiver with a parallel resonant tank achieves higher voltages and lower currents compared to a series resonant tank. Higher quality factor of resonant tank increases maximal voltage in parallel resonant tank and maximal current in series resonant tank. Very low values of coupling coefficient ($k = 0.001$ to 0.01) correspond to loosely coupled WPT with high degree of movement and positioning freedom for the receiver. The voltage generated at the receiver varies significantly with receiver's position (due to coupling coefficient) and quality factor of the resonant tank.

The variations in generated voltage can easily span over an order of magnitude. In such operating conditions, the parallel resonant tank is more suitable as a power source 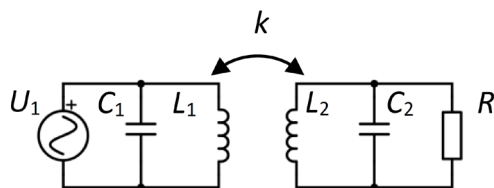for WSN. Higher output voltages (compared to series resonant tank) allow for simpler energy management design, and also for an increased operating range.

2.1 Energy Management Topology

The basic topology for the proposed energy management in WPT receiver is given in Fig. 2. It consists of three main building blocks: charge pump, energy storage and cold-start switching circuit.

The resonant tank of the WPT receiver is directly connected to the charge pump. Low ac voltage generated from the resonant tank is then converted to a higher dc voltage. Charge pump output is connected to the storage capacitor which acts as an energy storage. Due to large capacitance value and limited current from the charge pump, storage capacitor charging takes time. The voltage across the storage capacitor is monitored by a cold-start switching circuit.

When the voltage reaches a predefined value (turn-ON voltage level), the switching circuit connects the load to the storage capacitor. The load, whose current demand is higher than the output current of the charge pump, then starts to discharge the storage capacitor. When the voltage across storage capacitor drops down to a predefined value (turn-OFF voltage level), the load is disconnected. The voltage waveforms across the resonant tank, storage capacitor and load circuit are given in Fig. 2.

This way, the WPT receiver with low voltage and current drivability, can be used to power the load circuit which requires higher voltage and current levels. The load circuit operates in discontinuous mode, with long inactive time intervals and short active time intervals corresponding to charging and discharging of storage capacitor.

The following sections will discuss how to optimize all three main building blocks of energy management (charge pump, energy storage, and cold-start switching circuit) with emphasis on cold-start switching circuit design.

2.2 Charge Pump

The simplest method to boost ac voltage from the WPT receiver to a higher dc voltage is using a charge pump. Dickson charge pump requires no additional control signals and it works well with low current power source. Figure 3
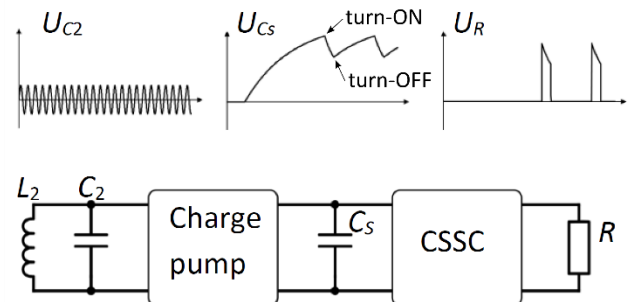
Fig. 2. Energy management topology for parallel WPT receiver.

Fig. 1. WPT system.

shows the schematic of Dickson charge pump. Dickson charge pumps consist of diodes (or diode-connected MOSFETs) and capacitors. In the proposed application the output capacitor (C_{out}) of Dickson charge pump is storage capacitor (see Fig. 2). In Fig. 3 the resonant tank is replaced with Thevenin equivalent circuit (U_{EH}, R_{EH}).

When the Dickson charge pump is used with an energy harvester source or WPT receiver with low output current, the output resistance R_{EH} of the energy harvester (or resonant tank of the WPT receiver) has a significant role. It forms a low-pass filter with parasitic capacitance C_{PAR} at charge pump input (Fig. 3) which limits maximal frequency (f_{MAX}) at which the charge pump can operate. This upper cut-off frequency f_{MAX} is given as [14]:

$$f_{MAX} = \frac{1}{2\pi R_{EH} C_{PAR}} \text{ [Hz]}. \quad (1)$$

In loosely coupled WPT system, the R_{EH} value depends on the resonant tank of the receiver (values of capacitance and inductance, and the quality factor), and it does not change significantly with the coupling coefficient k. The operating frequency of the charge pump (which equals the operating frequency of WPT system) must be lower than the upper cut-off frequency f_{MAX}. Then, the stage capacitors C value can be selected as [14]:

$$C > \frac{N}{f_{MAX} \cdot F \cdot (N+1)^2 R_{EH}} \text{ [F]} \quad (2)$$

where F is the crest factor of the U_{EH} waveform, e.g. $F = 1.414$ for sine voltage waveform. Number of charge pump stages N depends on the diode's threshold voltage U_{th} and the difference between input voltage U_{EH} and output voltage U_0 of the charge pump [14]:

$$N = 2\left(\frac{U_0}{\hat{U}_{EH} - U_{th}} - 1 \right). \quad (3)$$

Factor 2 in (3) is needed to set the operating point of the charge pump to maximum power point (MPP). This also requires for load to match the output resistance of the charge pump. In the proposed topology of energy management in WPT receiver the charge pump has a capacitive load during charging phase.

Thus, the MPP cannot be achieved without additional circuitry. When MPP is not used, the number of charge pump stages can be cut in half, which significantly decreases charge pump output resistance R_{S_EH} [14], equation (4), and decreases storage capacitor charging time.
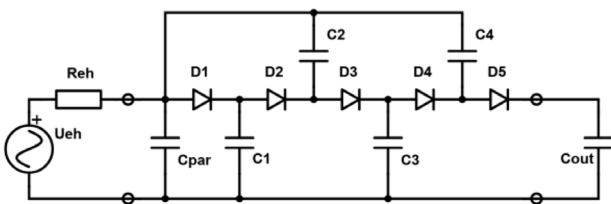
$$R_{S\_EH} = F \cdot (N+1)^2 \cdot R_{EH} + \frac{N \cdot f}{C} \text{ [}\Omega\text{]}. \quad (4)$$

In loosely coupled WPT system, the charge pump input voltage can vary over an order of magnitude. The number of charge pump stages N should be such that the charge pump output voltage is sufficient for a minimal value of expected input voltage. For higher input voltage values, the storage capacitor will charge faster, resulting in more frequent discharge phases.

2.3 Storage Capacitor

A storage capacitor is connected to the output of the Dickson charge pump and its capacitance value depends on the load circuit. In charge/discharge operating mode, the storage capacitor must be able to supply the load circuit with required voltage and current levels for at least one operating cycle (for WSN node, one cycle is composed of data acquisition and transmission).

For the proposed energy management topology to be feasible, the size of the storage capacitor must be reasonable. To determine the needed capacitance of the storage capacitor, measurements of power consumption of WSN node using LoRa [5], [6] and Bluetooth [7] were performed. The measurements are done on Waspmote PRO v1.5, IoT solution developed by libelium, with two wireless interfaces: LoRa 868 (900/915 MHz) and Bluetooth Low Energy (BLE) 4.0, Fig. 4.

The power consumption of IoT device was measured by measuring battery current using Device Current Waveform Analyzer CX3324A. There are 10 different LoRa operation modes that can be selected on Waspmote IoT device. Mode 1 has a maximal range with a slow data rate. Mode 10 has a minimal range, a fast data rate and has a minimal battery impact. Based on the current profile measurements, the energy required to perform single transmission is given in Fig. 5. The values range from 200 mJ down to 4 mJ.

Fig. 3. Dickson charge pump.

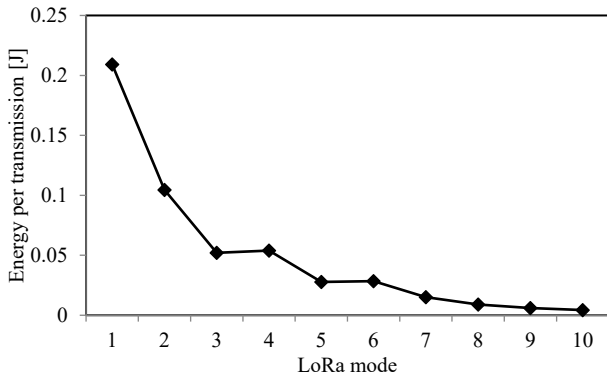**Fig. 4.** LoRa and BLE modules with Waspmote PRO v1.5.

Fig. 5. Energy per transmission for different LoRa operation modes.
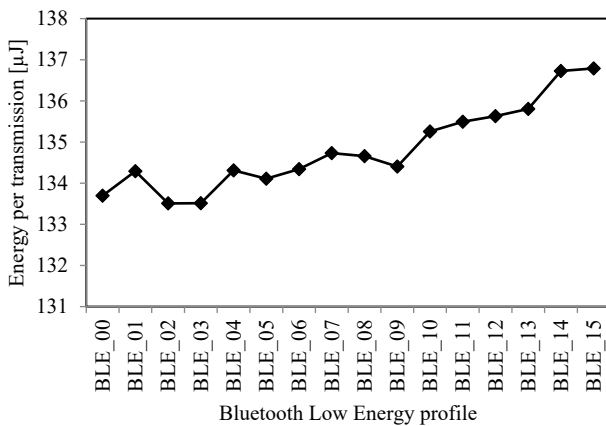

Fig. 6. Energy per transmission for BLE with different power profiles.

Bluetooth module available with Waspmote PRO v1.5 has adjustable transmitting power with 16 different power profiles (0–15). The current consumption for different power profiles was measured and the values of energy required for a single transmission are given in Fig. 6.

With higher output power (–23 dBm for BLE_00 to +3 dBm for BLE_15; from datasheet) the energy required for single transmission increases, but the overall energy increase is under 3%. Based on measured energy required for a single transmission, a needed storage capacitor size ranges from 40 µF for BLE, up to 2–60 mF for LoRA.

3. Cold-Start Switching Circuit

The proposed switching circuit combines two features, cold-start and energy-aware voltage monitoring/switching. Schematic is given in Fig. 7. W/L ratios for each MOSFET are given in brackets in Fig. 7. Capacitor C_1 is the storage capacitor, and resistor R_3 represents the load circuit.

The storage capacitor charges through the charge pump, and when it reaches a sufficient voltage (turn-ON voltage), the switch P_{10} connects the load circuit to the storage capacitor. The energy management circuit continues to monitor the voltage across the capacitor and when it drops to a predefined value (turn-OFF voltage), P_{10} disconnects the load. The power consumption of switching circuit is regulated by two external trimmer resistors (R_1 and R_2) used by PMOS and NMOS current mirrors. R_1 and R_2 are also used to set turn-ON and turn-OFF voltage values (for ON trigger and OFF trigger in Fig. 7).
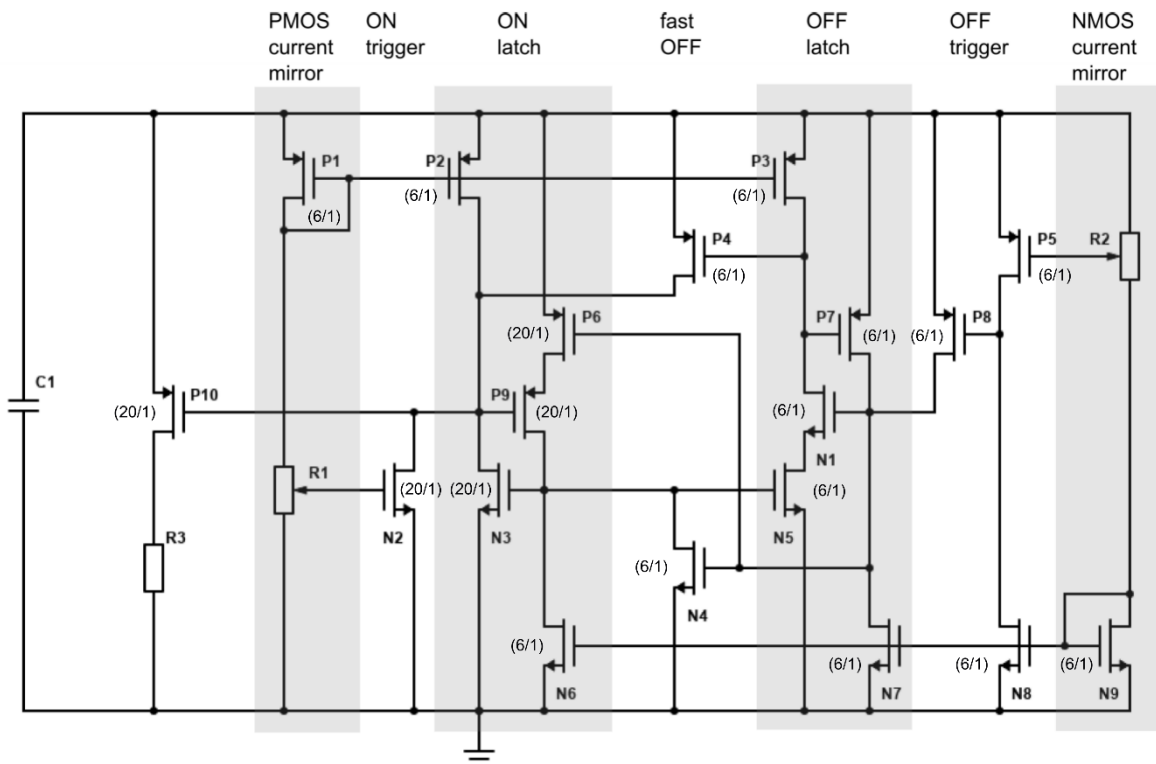

Fig. 7. Cold-start switching circuit.

The proposed design of the energy management circuit has a cold start feature which is essential for a battery-less devices. For an application in WPT system, wireless power transfer can be used on demand. For example, a WPT system is engaged only when a new data acquisition is required from WSN node. During longer time intervals without power supply the storage capacitor discharges completely. When the power supply is restored, the storage capacitor starts charging from 0 V. It is important to notice that the switching circuit is supplied from the storage capacitor, meaning that its "supply voltage" ranges from 0 V to load turn-ON voltage (2–3 V).

With a limited input current, storage capacitor charging takes time. Depending on the input current and storage capacitor size, the charging time can be up to few minutes. During this time, the load must be disconnected from the storage capacitor, and the power consumption of the switching circuit should be kept as low as possible.

The voltage waveforms of the voltage across the storage capacitor and load circuit are given in Fig. 8. When the WPT system is powering the WPT receiver, the voltage across the storage capacitor starts to increase from 0 V. There are two thresholds defined: turn-ON voltage and turn-OFF voltage. When the voltage across the storage capacitor reaches the turn-ON voltage, the energy management circuit connects the load circuit to the storage capacitor. Due to higher current demand from the load circuit, the voltage across the storage capacitor starts to decrease until it drops to the turn-OFF voltage value. Then the energy management circuit disconnects the load circuit and the storage capacitor charges for another operating cycle. The load circuit is connected to the storage capacitor through PMOS P_{10}, and because of the voltage drop on P_{10}, the voltage across the load circuit is lower than the voltage across the storage capacitor. The maximal and minimal load voltage values are marked as load-ON voltage and load-OFF voltage in Fig. 8.

The time diagram of the state of MOSFET switches (on/off) is given in Fig. 9. For each MOSFET, the low level indicates that the MOSFET is turned off (open switch), while the high level indicates a closed switch (turned on). In addition, there are fast and slow switching events, which are depicted with the slope of the transition between on and off states. Vertical lines are fast switching events and slopes with 45-degree angle are slow switching events.
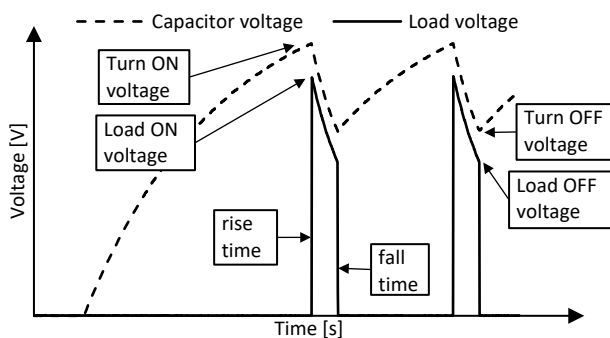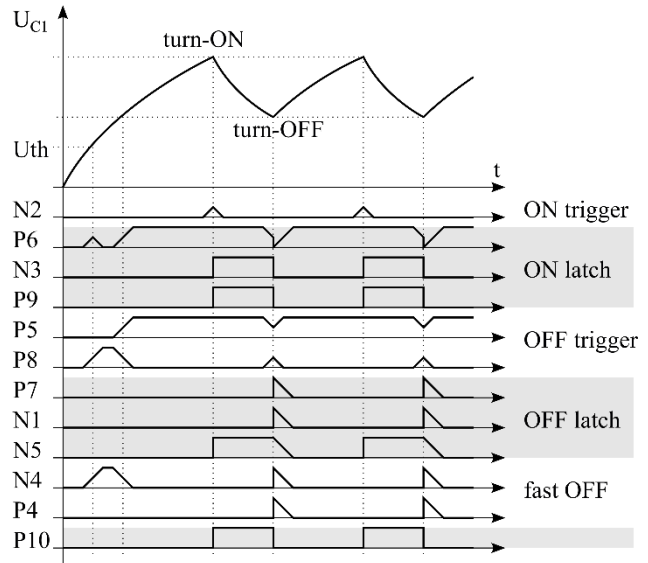

Fig. 9. Time diagram of MOSFET switches.

The turn-ON threshold voltage value is adjusted by trimmer resistor R_1. When the turn-ON voltage is reached, the N_2 (ON trigger) starts conducting. It triggers the ON latch which ensures fast and reliable switching event. P_9 starts conducting, it turns N_3 on, which results with P_9 and N_3 keeping each other in conduction.

A similar scheme is used for the turn-OFF threshold voltage. When the voltage across the storage capacitor drops down to the turn-OFF voltage, the OFF-trigger triggers OFF-latch. OFF-latch turns on (P_7 and N_1), and then fast-OFF circuit (P_4, N_4) discharges the transistor gates in ON-latch, resulting in a fast disconnection of the load circuit. In the previous designs of the energy management circuit [15–17], a fast switching while disconnecting the load circuit was found to be important in order to ensure proper operation and functionality of the energy management circuit.

To keep ON-latch and OFF-latch from misfiring, additional "enable" MOSFET is added to both latches (P_6 in ON-latch, N_5 in OFF-latch). They ensure that each latch can only be triggered during a correct time interval, e.g. the OFF-latch can turn on only after the ON-latch is in conduction. This is important because the turn-OFF threshold voltage is lower than the turn-ON threshold voltage.

4. Measurements

The proposed cold-start switching circuit (CSSC) is designed and fabricated in 180 nm TSMC CMOS technology. Figure 10 shows the test setup with CSSC soldered on a PCB test board. The CSSC requires two external components: trimmer resistors R_1 and R_2. Due to large resistance values and the need to fine-tune the turn-ON and turn-OFF threshold voltage values, external trimmer resistors were chosen. All the transistors shown in Fig. 7 are integrated, including the main switch P_{10}. The load resistor and the storage capacitor are also marked in Fig. 10. The resonant tank and the charge pump are for testing purposes replaced by DC power

Fig. 8. Storage capacitor and load circuit voltage waveforms.

supply with series resistance (an equivalent Thevenin voltage source UEH and resistor REH). Three sets of measurements were done to evaluate the performance of the fabricated cold-start switching circuit: power consumption, switching characteristics and the performance during external circuit (WSN node) powering.

4.1 Power Consumption

To evaluate the power consumption of the switching circuit, the load resistor was disconnected from the PCB test board. Then, the voltage across the storage capacitor was varied from 0 V up to the turn-ON voltage level, and back down to the voltage level below the turn-OFF voltage. During this time, the current consumption of the switching circuit was measured. Voltage is varied in steps of 0.1 V (measurement steps in Fig. 11). The current consumption of the switching circuit depends on the resistance of the trimmer resistors (R_1 and R_2) which are used to set the current reference for PMOS and NMOS current mirrors.

The current consumption measurements are done for trimmer resistor values $R_1 = R_2 = 5$ MΩ and $R_1 = R_2 = 100$ MΩ, Fig. 11. Current consumption has almost linear dependence to the storage capacitor voltage with higher consumption level during discharging phase. For a CSSC with 100 MΩ trimmer resistors and the turn-ON voltage level of 2.7 V, the maximal current during the charging phase is 350 nA, resulting with maximal power consumption of 0.945 μW. Table 1 gives the comparison of the proposed cold-start switching circuit to the state-of-the-art with respect to power consumption which is a main figure of merit (FoM). The proposed solution is comparable to the best state-of-the-art solutions in terms of power consumptions.
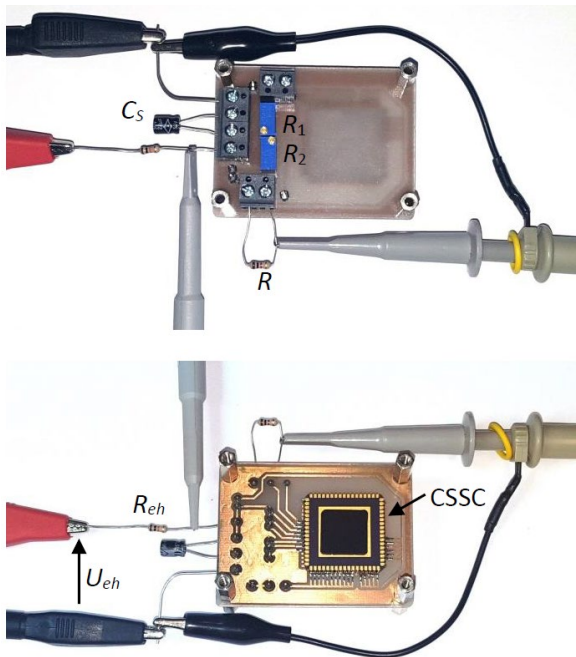

Fig. 10. Fabricated cold-start switching circuit soldered on a PCB test board: (a) top view and (b) bottom view.
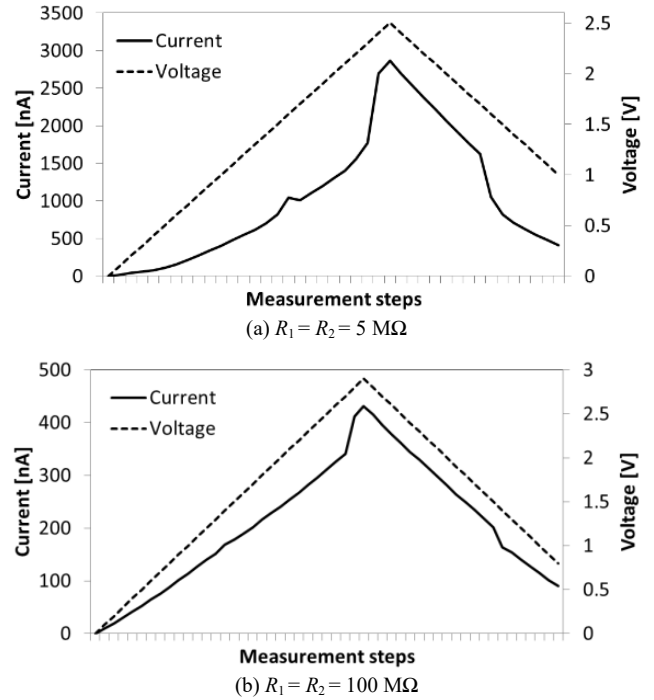

(a) $R_1 = R_2 = 5$ MΩ

(b) $R_1 = R_2 = 100$ MΩ

Fig. 11. Current consumption profiles of switching circuit with trimmer resistor values: (a) 5 MΩ and (b) 100 MΩ.

Paper	Power consumption	Year	Technology
This work	0.945 μW	2022	180 nm CMOS
[18]	0.905 μW	2021	180 nm CMOS
[19]	2.68 μW	2020	discrete
[20]	1.35 μW	2020	0.35 μm CMOS
[21]	0.67 μW	2019	180 nm CMOS
[8]	7.39 μW	2018	65 nm CMOS
[9]	0.667 μW	2018	180 nm CMOS
[22]	15.54 μW	2018	discrete
[23]	16 μW	2013	65 nm CMOS

Tab. 1. Power consumption comparison with state-of-the-art.

4.2 Switching Characteristics

The turn-ON and turn-OFF threshold voltage levels are set with trimmer resistors. Once the voltage across the storage capacitor reaches the threshold voltage level, the trigger section (ON-trigger and OFF-trigger in Fig. 7) of the CSSC activates. For that to happen, a certain time interval is required. For example, activated OFF-trigger equals to non-conducting PMOS P_8. For P_8 to stop conducting its gate must discharge through current mirror N_8, whose current depends on the trimmer resistor R_2 value. Simplified, the time constant formed with trimmer resistor R_2 and C_{GS} capacitance of P_8 defines the response time of the OFF-trigger. The same logic can be applied to the ON-trigger, where the response time is defined by the time constant formed with trimmer resistor R_1 and C_{GS} capacitance of N_2. C_{GS} value is approximately 500 fF for the used 180 nm TSMC CMOS technology.

To have stable threshold voltage values, the durations of charging and discharging phases must be at least five

times longer than the time constants of ON- and OFF-trigger. To evaluate threshold voltage level stability, threshold voltage levels were measured for different capacitance values of the storage capacitor (from 680 pF to 1 µF). With fixed values of R_{EH} (100 kΩ) and R_{load} (10 kΩ), different storage capacitors result with different charging and discharging times. Results are given in Fig. 12.

It can be seen that for the charging/discharging times longer than 100 µs, the threshold voltage levels are stable. For an intended use of the CSSC, charging/discharging times are at least 3 orders of magnitude longer, so this border case would not be reached. But, the minimal charging/discharging time increases with higher values of R_1 and R_2 (lower power consumption of CSSC). This is a trade-off that should be taken into consideration.

Transition between charging and discharging phase is evaluated by measuring rise and fall time of the voltage across the load resistor, Fig. 8. The load resistor has the major influence on the rise and fall time. Measurement results are shown in Fig. 13. Load resistance has a small impact on the rise time and a significant impact on the fall time. The fall time has a linear correlation to the load resistance. For lower values of the load resistances, the rise and fall time are under 100 ns.

The load-ON voltage (Fig. 8) is lower than the turn-ON voltage. The same goes for the load-OFF voltage and the turn-OFF voltage. This difference is due to a voltage drop
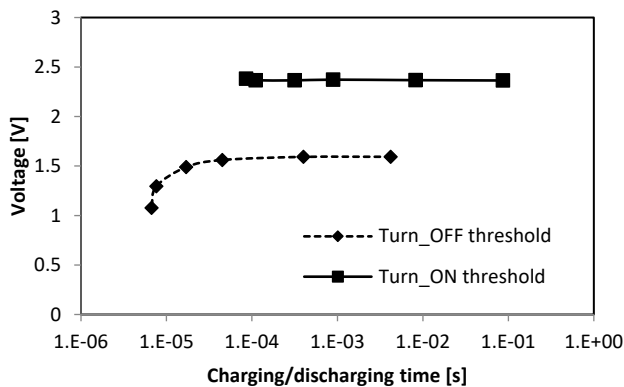
across the switch (P_{10} in Fig. 7) and it should be as small as possible. The voltage drop across the switch directly reduces the overall efficiency. With integrated switch P_{10}, for load currents of 20 µA, 200 µA and 2 mA, the measured voltage drop across the switch equals 30 mV, 100 mV and 900 mV, respectively. For higher load currents, an external switch should be used.

4.3 WSN Node Powering

To power a WSN node, instead of the internal MOSFET P_{10}, an external MOSFET (SUP53P06-20) is used as a switch between the storage capacitor and the WSN node. In Sec. 2.3, an energy required for a single transmission is measured. The values are given for LoRa and Bluetooth wireless interface. Each single transmission is relatively short in duration (1 ms for Bluetooth and 100 ms for LoRa), and based on durations of single transmission, the required storage capacitor values are calculated. When the WSN node is powered through the cold-start switching circuit, each time it turns on, the WSN node start-up/initialization is performed.

For the Waspmote PRO v1.5, the initialization takes approximately 3 seconds to complete, and only then the data transmission takes place. Therefore, a larger capacitor is needed for one operating cycle. Figure 14 shows the measurement setup for the WSN node powered through the cold-start switching circuit. For the testing purposes 1 F supercapacitor is used in addition to a 2200 µF electrolytic capacitor. The turn-ON and turn-OFF threshold voltage are set to 3.25 and 3 V, respectively. With 1 F storage capacitor, active interval of the WSN node is approximately 8 seconds long, Fig. 15. During that time, the WSN node performs initialization and several data transmissions. When the CSSC connects the WSN to the storage capacitor, a large inrush current is measured with values exceeding 1 A, Fig. 15. This is significantly higher compared to average WSN current of 30 mA.

Due to large inrush current, the voltage drop on the ESR of the supercapacitor lowers the storage capacitor voltage below the turn-OFF threshold voltage. This results with unwanted behavior during the turn-ON transition, Fig. 16(a). Voltage waveforms on WSN node have a comb-like shape and the turn-ON transition takes two orders of

Fig. 12. Turn-ON and turn-OFF threshold voltage levels for different charging/discharging times, $R_1 = R_2 = 5$ MΩ.
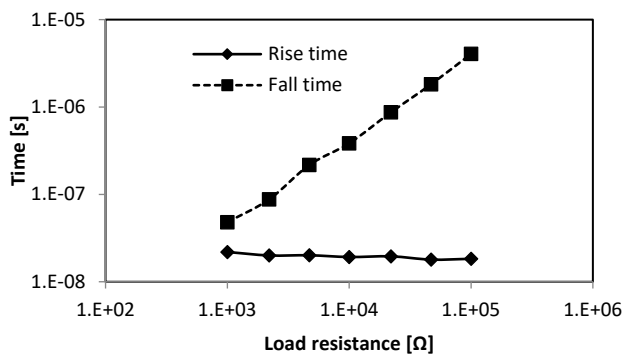

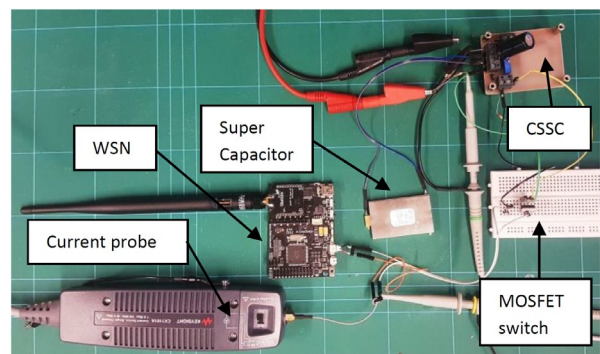**Fig. 13.** Rise and fall time of the load voltage for different load resistor values.

Fig. 14. WSN powered through CSSC - measurement setup.
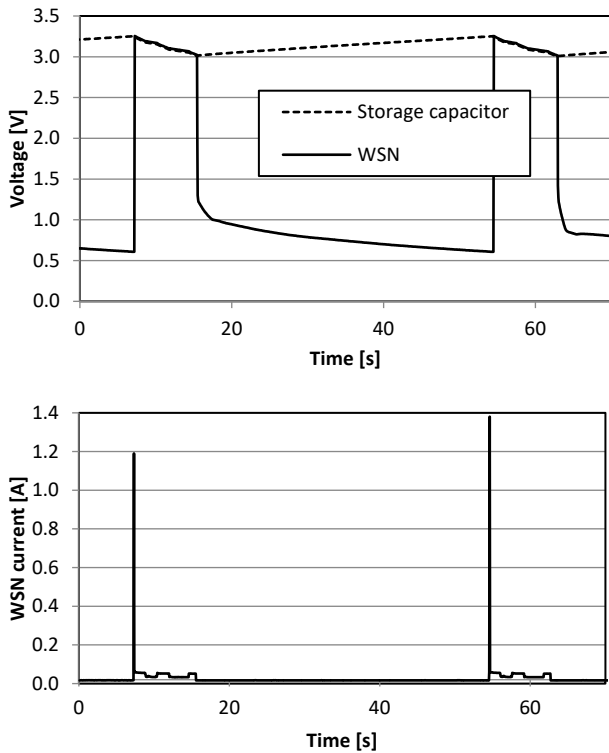
Fig. 15. Voltage and current waveforms for WSN node powered through CSSC.

(a) without electrolytic capacitor
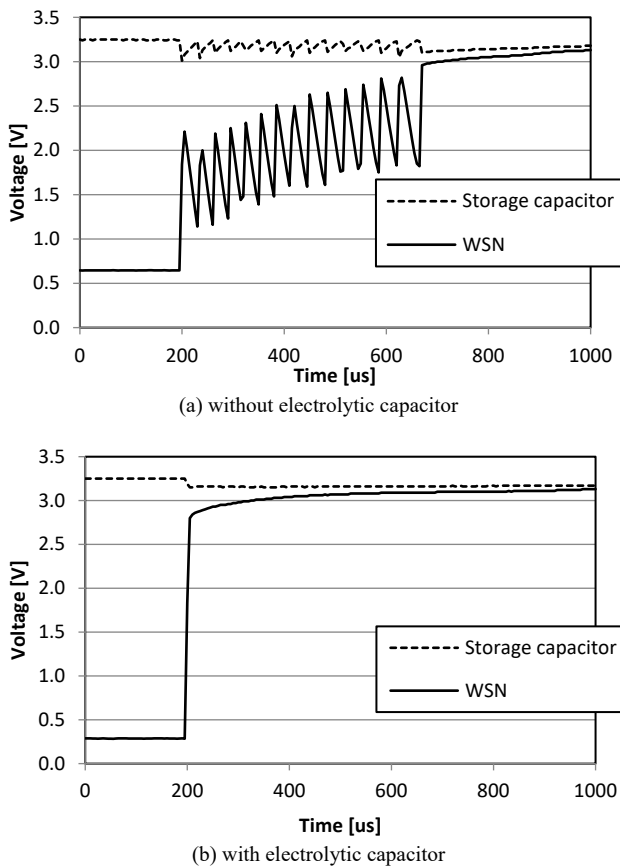

(b) with electrolytic capacitor

Fig. 16. Turn-ON transition voltage waveforms without (a) and with (b) supercapacitor.

magnitude longer. To cope with this problem, an electrolytic capacitor (2200 µF) is added in parallel to the supercapacitor, Fig. 16(b).

5. Conclusion

Energy management topology suitable for wireless power transfer systems is proposed. The proposed topology consists of three sub-circuits: charge pump, storage capacitor and cold-start switching circuit. Design and optimization of the charge pump and storage capacitor are briefly described. The main emphasis is on the cold-start energy-aware switching circuit. The circuit is designed to operate in discontinuous mode to power load circuits which require higher voltage and current levels than available from the WPT receiver. The proposed cold-start switching circuit is designed and fabricated in 180 nm TSMC CMOS technology. Measurements on the prototype have shown that the cold-start switching circuit has low power consumption (less than 1 µW), stable turn-ON and turn-OFF threshold voltage levels which can be adjusted, and fast switching times. The cold-start switching circuit can be used to drive external power MOSFET required for load circuits with higher current demand. This was successfully tested with WSN node powered through the developed cold-start switching circuit. The proposed design is a versatile solution for energy-aware switching circuits with cold-start functionality.

Acknowledgments

References

[1] MA, D., LAN, G., HASSAN, M., et al. Sensing, computing, and communications for energy harvesting IoTs: A survey. *IEEE Communications Surveys & Tutorials*, 2020, vol. 22, no. 2, p. 1222 to 1250. DOI: 10.1109/COMST.2019.2962526

[2] RUAN, T., CHEW, Z. J., ZHU, M. Energy-aware approaches for energy harvesting powered wireless sensor nodes. *IEEE Sensors Journal*, 2017, vol. 17, no. 7, p. 2165–2173. DOI: 10.1109/JSEN.2017.2665680

[3] AZARHAVA, H., NIYA, J. M. Energy efficient resource allocation in wireless energy harvesting sensor networks. *IEEE Wireless Communications Letters*, 2020, vol. 9, no. 7, p. 1000–1003. DOI: 10.1109/LWC.2020.2978049

[4] ZHANG, H., GUO, Y.-X., ZHONG, Z., et al. Cooperative integration of RF energy harvesting and dedicated WPT for wireless sensor networks. *IEEE Microwave and Wireless Components Letters*, 2019, vol. 29, no. 4, p. 291–293. DOI: 10.1109/LMWC.2019.2902047

[5] CROCE, D., GUCCIARDO, M., MANGIONE, S., et al. LoRa technology demystified: From link behavior to cell-level

performance. *IEEE Transactions on Wireless Communications*, 2020, vol. 19, no. 2, p. 822–834. DOI: 10.1109/TWC.2019.2948872

[6] SUNDARAM, J. P. S., DU, W., ZHAO, Z. A survey on LoRa networking: Research problems, current solutions and open issues. *IEEE Communications Surveys & Tutorials*, 2020, vol. 22, no. 1, p. 371–388. DOI: 10.1109/COMST.2019.2949598

[7] JEON, K. E., SHE, J., SOONSAWAD, P., et al. BLE beacons for Internet of Things applications: Survey, challenges, and opportunities. *IEEE Internet of Things Journal*, 2018, vol. 5, no. 2, p. 811–828. DOI: 10.1109/JIOT.2017.2788449

[8] LUO, Z., ZENG, L., LAU, B., et al. A sub-10 mV power converter with fully integrated self-start, MPPT, and ZCS control for thermoelectric energy harvesting. *IEEE Transactions on Circuits and Systems I: Regular Papers*, 2018, vol. 65, no. 5, p. 1744–1757. DOI: 10.1109/TCSI.2017.2757505

[9] BOSE, S., ANAND, T., JOHNSTON, M. L. Fully-integrated 57 mV cold start of a thermoelectric energy harvester using a cross-coupled complementary charge pump. In *Proceedings of 2018 IEEE Custom Integrated Circuits Conference (CICC)*. San Diego (CA, USA), 2018, p. 1–4. DOI: 10.1109/CICC.2018.8357081

[10] DEZYANI, M., GHAFOORIFARD, H., SHEIKHAEI, S., et al. A 60 mV input voltage, process tolerant start-up system for thermoelectric energy harvesting. *IEEE Transactions on Circuits and Systems I: Regular Papers*, 2018, vol. 65, no. 10, p. 3568–3577. DOI: 10.1109/TCSI.2018.2834312

[11] BOSE, S., ANAND, T., JOHNSTON, M. L. A 3.5mV input, 82% peak efficiency boost converter with loss-optimized MPPT and 50mV integrated cold-start for thermoelectric energy harvesting. In *Proceedings of 2019 IEEE Custom Integrated Circuits Conference (CICC)*. Austin (TX, USA), 2019, p. 1–4. DOI: 10.1109/CICC.2019.8780352

[12] YU, H., CHEN, M., WU, C., et al. A batteryless and single-inductor DC-DC boost converter for thermoelectric energy harvesting application with 190mV cold-start voltage. In *Proceedings of 2018 IEEE International Symposium on Circuits and Systems (ISCAS)*. Florence (Italy), 2018, p. 1–4. DOI: 10.1109/ISCAS.2018.8351428

[13] COUSTANS, M., KRUMMENACHER, F., KAYAL, M. A fully integrated 60 mV cold-start circuit for single coil DC–DC boost converter for thermoelectric energy harvesting. *IEEE Transactions on Circuits and Systems II: Express Briefs*, 2019, vol. 66, no. 10, p. 1668–1672. DOI: 10.1109/TCSII.2019.2922683

[14] VINKO, D. Applicability of Dickson charge pump in energy harvesting systems: Experimental validation of energy harvesting charge pump model. *Radioengineering*, 2018, vol. 27, no. 2, p. 510 to 518. DOI: 10.13164/re.2018.0510

[15] VINKO, D. Minimizing switching time of energy harvesting management circuit. In *Proceedings of 41st International Convention on Information and Communication Technology, Electronics and Microelectronics (MIPRO)*. Opatija (Croatia), 2018, p. 0099–0102. DOI: 10.23919/MIPRO.2018.8400019

[16] VINKO, D. Power management circuit for energy harvesting applications with zero-power charging phase. In *Proceedings of 40th International Convention on Information and Communication Technology, Electronics and Microelectronics (MIPRO)*. Opatija (Croatia), 2017, p. 158–161. DOI: 10.23919/MIPRO.2017.7973409

[17] VINKO, D., HORVAT, G. 100 nA power management circuit for energy harvesting devices. In *Proceedings of 37th International Convention on Information and Communication Technology, Electronics and Microelectronics (MIPRO)*. Opatija (Croatia), 2014, p. 125–129. DOI: 10.1109/MIPRO.2014.6859546

[18] TRAN-DINH, T., PHAM, H. M., PHAM-NGUYEN, L., et al. Power management IC with a three-phase cold self-start for thermoelectric generators. *IEEE Transactions on Circuits and Systems I: Regular Papers,* 2021, vol. 68, no. 1, p. 103–113. DOI: 10.1109/TCSI.2020.3023252

[19] MAYER, P., MAGNO, M., BENINI, L. A low power and smart power unit for kinetic self-sustainable wearable devices. In *2020 27th IEEE International Conference on Electronics, Circuits and Systems (ICECS)*. Glasgow (UK), 2020, p. 1–4. DOI: 10.1109/ICECS49266.2020.9294783

[20] BESSAAD, A., RHOUNI, A., BASSET, P., et al. Power management integrated circuit for electrostatic kinetic energy harvesters. In *2020 IEEE International Symposium on Circuits and Systems (ISCAS)*. Seville (Spain), 2020, p. 1–5. DOI: 10.1109/ISCAS45731.2020.9180972

[21] BOSE, S., ANAND, T., JOHNSTON, M. L. Integrated cold start of a boost converter at 57 mV using cross-coupled complementary charge pumps and ultra-low-voltage ring oscillator. In *IEEE Journal of Solid-State Circuits*, 2019, vol. 54, no. 10, p. 2867–2878. DOI: 10.1109/JSSC.2019.2930911

[22] GÖTZ, M., KANOUN, O. Ultralow power voltage supervisor for ambient power-driven microcontroller systems. *IEEE Transactions on Industrial Electronics*, 2019, vol. 66, no. 5, p. 3843–3851. DOI: 10.1109/TIE.2018.2851981

[23] WENG, P.-S., TANG, H.-Y., KU, P.-C., et al. 50 mV-input batteryless boost converter for thermal energy harvesting. *IEEE Journal of Solid-State Circuits*, 2013, vol. 48, no. 4, p. 1031–1041. DOI: 10.1109/JSSC.2013.2237998

About the Authors ...

Davor VINKO (corresponding author) received his M.Sc. and Ph.D. degree from J. J. Strossmayer University of Osijek, Faculty of Electrical Engineering, in 2005 and 2012, respectively. Currently he is an Associate Professor at the Faculty of Electrical Engineering, Computer Science and Information Technology in Osijek (Department of Communications). His main research interests include charge pumps, energy harvesting circuits and wirelessly powered devices.

Krešimir GRGIĆ received his M.Sc. and Ph.D. degree from J. J. Strossmayer University of Osijek, Faculty of Electrical Engineering, in 2005 and 2011, respectively. Currently he is an Associate Professor at the Faculty of Electrical Engineering, Computer Science and Information Technology in Osijek (Department of Communications). His main research interests include communication networks and wireless sensor networks, with focus on cybersecurity aspects. He is a senior member of IEEE.

Domagoj BILANDŽIJA is an Assistant at the Faculty of Electrical Engineering, Computer Science and Information Technology Osijek, J. J. Strossmayer University of Osijek, Croatia. He received master's degree in Electrical Engineering from the Faculty of Electrical Engineering Osijek in 2017 and he is currently working toward a Ph.D. degree in Electrical Engineering at the Faculty of Electrical Engineering, Computer Science and Information Technology Osijek. His studies focus on wireless power transfer and optimization methods.